IOPscience iopscience.iop.org

Home Search Collections Journals About Contact us My IOPscience

Magnetism in $FeNb_2O_6$ and $NiNb_2O_6$

This article has been downloaded from IOPscience. Please scroll down to see the full text article.

1996 J. Phys.: Condens. Matter 8 10609

(http://iopscience.iop.org/0953-8984/8/49/046)

View the table of contents for this issue, or go to the journal homepage for more

Download details:
IP Address: 171.66.16.207
The article was downloaded on 14/05/2010 at 05:51

Please note that terms and conditions apply.

J. Phys.: Condens. Matter **8** (1996) 10609–10625. Printed in the UK

Magnetism in $FeNb_2O_6$ and $NiNb_2O_6$

C Heid†, H Weitzel†, F Bourdarot‡, R Calemczuk‡, T Vogt§‖ and H Fuess†

† Fachgebiet Strukturforschung, Fachbereich Materialwissenschaft, Technische Hochschule, D-64287 Darmstadt, Germany

‡ Centre d'Etudes Nucléaires de Grenoble, F-38041 Grenoble, France

§ Institut Laue–Langevin, F-38042 Grenoble, France

Received 20 May 1996, in final form 20 September 1996

Abstract. Results of a neutron diffraction study on powder samples of $FeNb_2O_6$ and $NiNb_2O_6$ at 1.3 K and on a single crystal of flux-grown $FeNb_2O_6$ at 1.5 K are given. The magnetization and susceptibility of single crystals have been measured for both compounds from 2.0 K to room temperature. In addition a Mössbauer spectrum of $FeNb_2O_6$ was taken at 4.2 K, and the specific heat of $NiNb_2O_6$ has been measured from 0.5 K up to 25 K. $FeNb_2O_6$ and $NiNb_2O_6$ exhibit antiferromagnetic order below 4.9 K and 5.7 K, respectively, with a canted magnetic structure. The powder samples reveal two propagation vectors, $(0\ \frac{1}{2}\ 0)$, and $(\frac{1}{2}\ \frac{1}{2}\ 0)$, for $FeNb_2O_6$ as well as for $NiNb_2O_6$. The magnetization measurements are interpreted in the mean-field approximation by taking the crystal field, spin–orbit coupling, isotropic Heisenberg exchange, magnetic dipole–dipole interaction and an external field into account. Within this model very good agreement between theory and experiment was obtained. By reproducing the antiferromagnetic–paramagnetic phase transitions with an applied external field parallel to the *a*- or *c*-direction an estimation of the effective exchange interaction between zigzag chains running along the *c*-direction is given. The magnetic structures, as derived from model considerations, agree with neutron diffraction results.

1. Introduction

The transition metal niobates MNb_2O_6 (M = Ni, Co, Fe, Mn) and $MnTa_2O_6$ crystallize in the columbite structure [1]. This crystal structure consists of layers of slightly distorted hexagonal-closed-packed oxygen octahedra perpendicular to the *a*-axis. Within each *b*–*c* layer, octahedra filled with cations are aligned in zigzag chains running along the *c*-axis with common edges. From layer to layer the cations within the octahedra alternate in the sequence M–Nb–Nb–M–Nb–Nb–M. The space group is $Pbcn$ (D_{2h}^{14}).

The antiferromagnetic structures of $MnNb_2O_6$ [2–4], $CoNb_2O_6$ [5] and $MnTa_2O_6$ [3] have been studied previously by neutron diffraction studies of single crystals. Powder diffraction studies have also been performed on $FeNb_2O_6$ [2] and $NiNb_2O_6$ [6]. The results are collinear magnetic structures with propagation vectors $(0\ \frac{1}{2}\ 0)$. No deviation from a collinear structure could be detected. Magnetization studies and group theoretical considerations [7, 8] gave later evidence of such non-collinear canted magnetic structures for $FeNb_2O_6$ and $NiNb_2O_6$. In this paper we report on new neutron diffraction studies on powder and single-crystal samples, and specific heat measurements as well as theoretical and experimental magnetization studies on single crystals.

‖ Present address: Brookhaven National Laboratory, Upton, NY 11973, USA.

0953-8984/96/4910609+17$19.50 © 1996 IOP Publishing Ltd

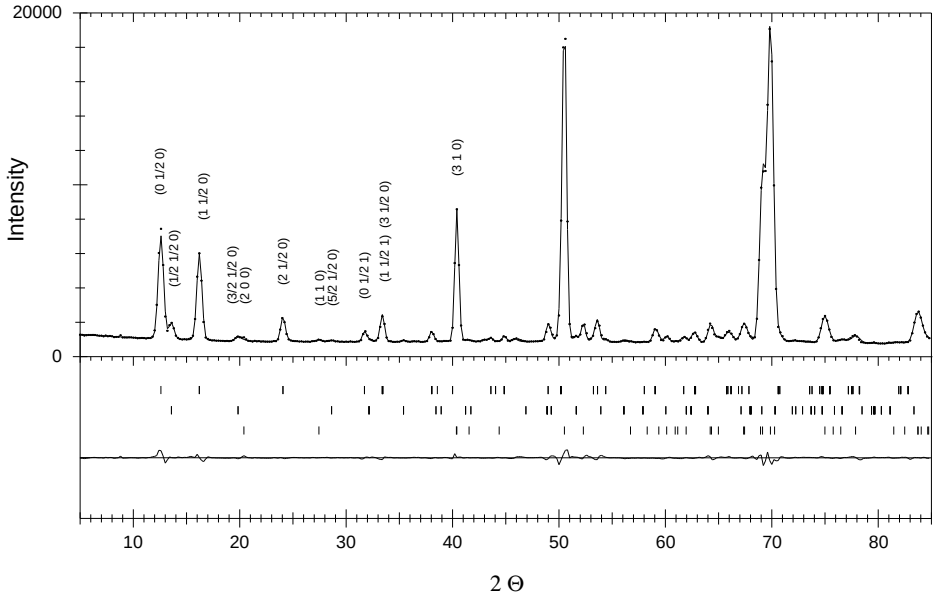

Figure 1. Observed and calculated diffraction patterns at 1.3 K for $FeNb_2O_6$. The first line of tick marks belong to magnetic reflections for the propagation vector (0 $\frac{1}{2}$ 0), the second to those for ($\frac{1}{2}$ $\frac{1}{2}$ 0) and the third to the nuclear reflections.

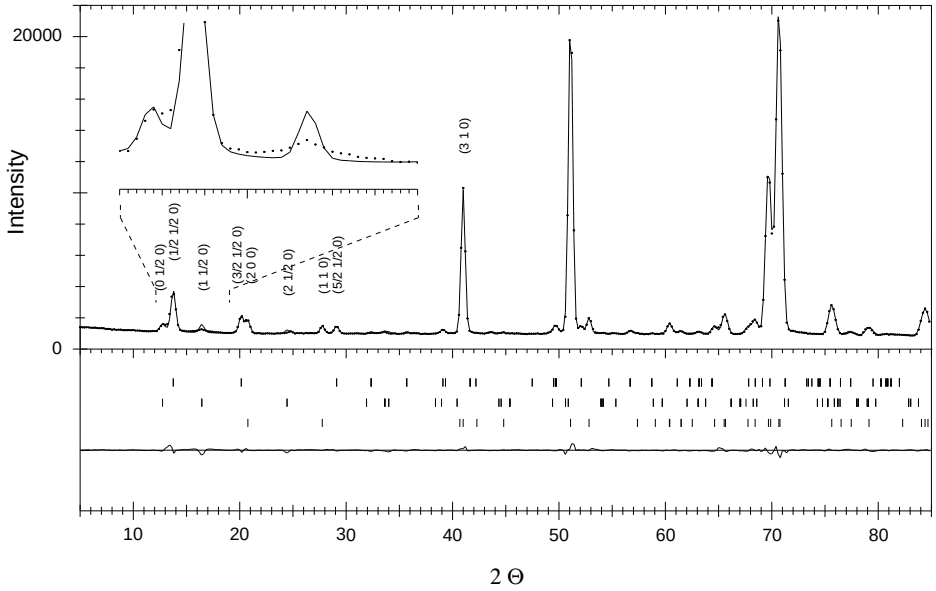

Figure 2. Observed and calculated diffraction patterns at 1.3 K for $NiNb_2O_6$. The first line of tick marks belong to magnetic reflections for the propagation vector ($\frac{1}{2}$ $\frac{1}{2}$ 0), the second to those for (0 $\frac{1}{2}$ 0) and the third to the nuclear reflections. The inset shows the strongly broadened Lorentzian-shaped (1 $\frac{1}{2}$ 0) reflection.

Section 2 describes the experiments, section 3 provides the results from the neutron diffraction study and a specific heat measurement. In section 4 a theoretical calculation of the magnetic properties is given. In contrast to the publications mentioned above [7, 8] which were based on effective spin Hamiltonians, in this work the degrees of freedom of the orbital angular momentum are explicitly taken into account. The results are finally summarized in section 5.

2. Experimental procedure

The $FeNb_2O_6$ and $NiNb_2O_6$ powders were synthesized by standard subsolidus reactions [9]. The neutron powder diffraction experiments were performed at the D1B diffractometer of the ILL. The data were collected at a wavelength of $\lambda = 2.5293$ Å in an angular range $5^\circ \leqslant 2\Theta \leqslant 85^\circ$ in steps of 0.2° and in a temperature range from 1.3 K to room temperature. The patterns taken at 1.3 K are shown in figures 1 and 2. For the refinement of the magnetic structures the program FULLPROF [10] was applied. In addition to a $\lambda/2$ contribution of 0.11% and reflections of the vanadium container, a solid nitrogen impurity in the $FeNb_2O_6$ sample was detected and included in the refinement.

In order to confirm the powder diffraction results, further neutron diffraction experiments on a flux-grown crystal [11] of $FeNb_2O_6$ were carried out. The crystal dimensions were $2 \times 3 \times 6$ mm^3. The measurements were performed on the DN3 normal-beam instrument of the reactor SILOË at the CEN Grenoble with a wavelength of 1.54 Å at 1.6 K. An extinction correction following Becker and Coppens [12] was carried out, and for the refinement the program MINREF [13] was used.

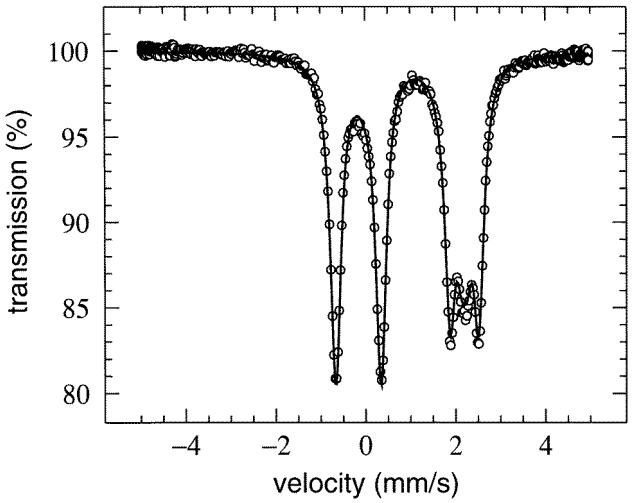

Figure 3. The observed and calculated Mössbauer spectra of $FeNb_2O_6$ at 4.2 K.

Mössbauer spectra of $FeNb_2O_6$, taken at 4.2 K and 77 K, were recorded by a conventional mechanical drive, synchronized with a multichannel analyser operating in time mode; see figure 3.

The specific heat of a $NiNb_2O_6$ single crystal was measured with an adiabatic heating calorimeter without field in the temperature range from 0.3 to 25 K; see figure 4.

The field-induced magnetization and susceptibility of the single crystals were measured

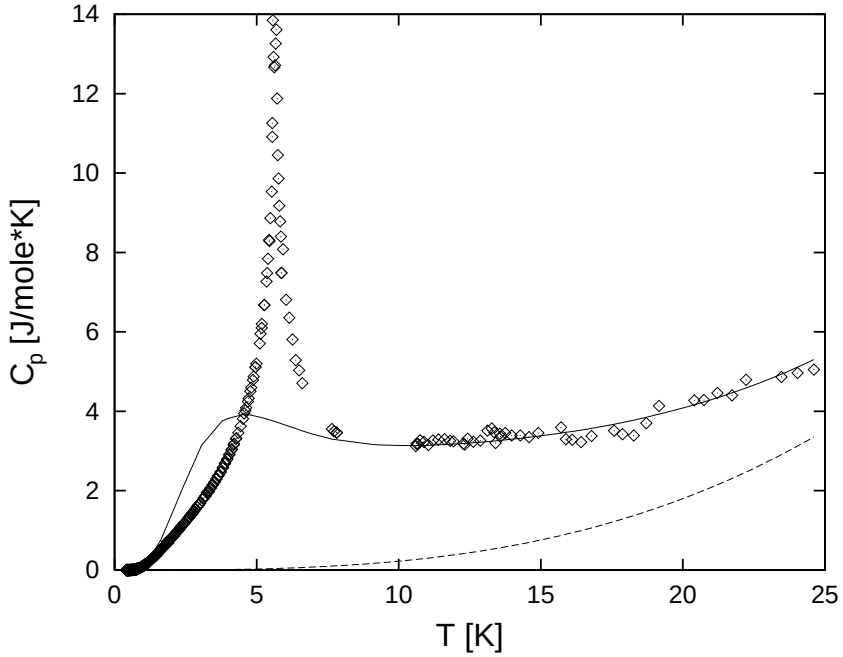

Figure 4. The specific heat of $NiNb_2O_6$. The solid line gives the theoretical prediction for a ferromagnetic $S = 1$ Heisenberg chain with uniaxial single-ion anisotropy. The dashed line gives the lattice contribution.

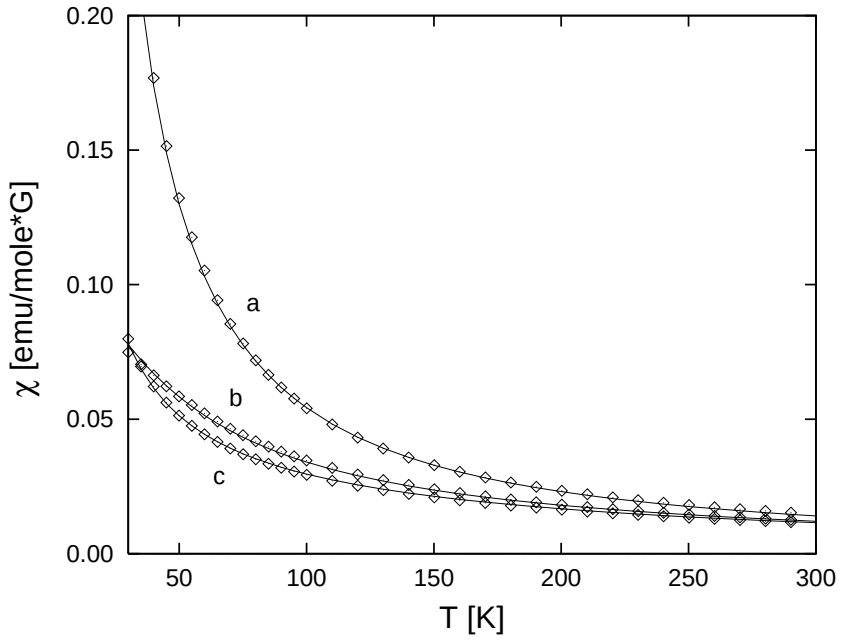

Figure 5. Magnetic susceptibilities of $FeNb_2O_6$ along the crystallographic axes a, b and c. The lines give the results of refinement.

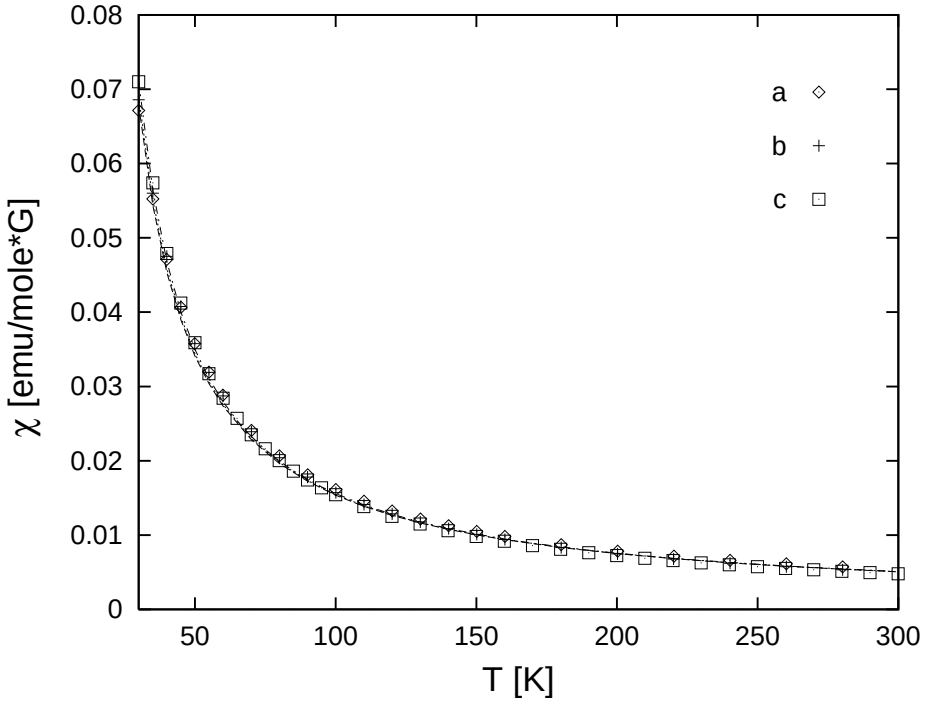

Figure 6. Magnetic susceptibilities of $NiNb_2O_6$ along the crystallographic axes *a*, *b* and *c*. The lines give the results of refinement.

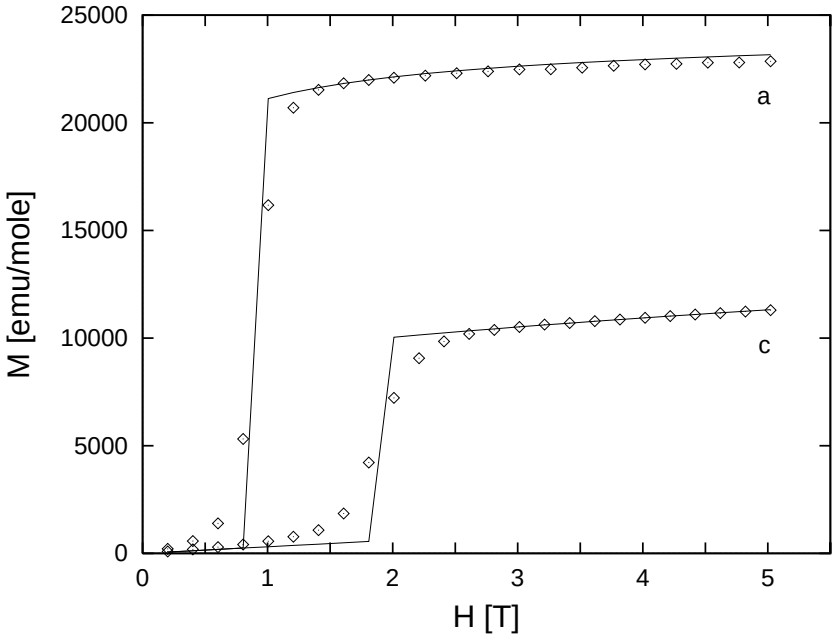

Figure 7. The magnetization of $FeNb_2O_6$ along the crystallographic axes *a* and *c* measured at 2.0 K. The lines give the results of refinement.

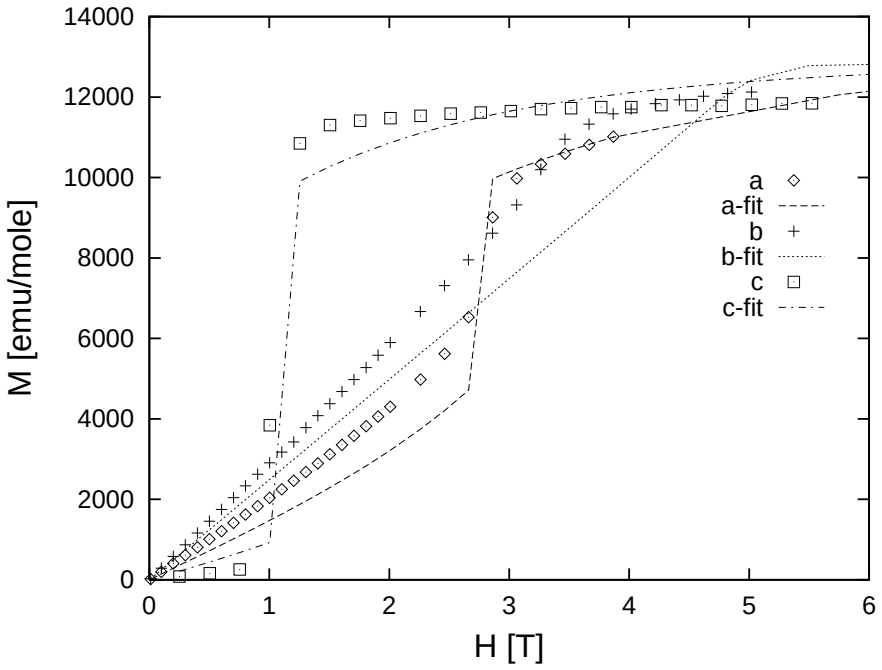

Figure 8. The magnetization of $NiNb_2O_6$ along the crystallographic axes *a*, *b* and *c* measured at 2.0 K. The lines give the results of refinement.

from 2 K to room temperature with a SQUID magnetometer (QUANTUM DESIGN). 'Susceptibility' here denotes the slope of the magnetization, which depends linearly on the applied field strength up to 100 G in the temperature range under consideration (figures 5 and 6). The field-dependent magnetizations were measured at 2.0 K and are shown in figures 7 and 8.

3. Results and discussion

The temperature-dependent powder diffraction experiments revealed antiferromagnetic order at 4.9 K and 5.7 K for $FeNb_2O_6$ and $NiNb_2O_6$ respectively. In addition to reflections with the propagation vector $(0\ \frac{1}{2}\ 0)$ [2, 6] we found further magnetic reflections, which could be indexed by a propagation vector $(\frac{1}{2}\ \frac{1}{2}\ 0)$; see figures 1 and 2. No change in the intensity of the nuclear reflections was observed. In $FeNb_2O_6$ the reflections belonging to the propagation vector $(0\ \frac{1}{2}\ 0)$ are more intense than those belonging to $(\frac{1}{2}\ \frac{1}{2}\ 0)$, whereas for $NiNb_2O_6$ the opposite was observed. As the most intense reflections, $(0\ \frac{1}{2}\ 0)$ and $(\frac{1}{2}\ \frac{1}{2}\ 0)$, corresponding to the two propagation vectors lie close together, they could not be separated in previous experiments due to the low resolution and the short wavelength used. Furthermore the reflections in $NiNb_2O_6$ belonging to the propagation vector $(0\ \frac{1}{2}\ 0)$ have a Lorentzian shape with increasing broadening for increasing 2Θ, indicating magnetic stacking faults presumably in the crystallographic *a*-direction. Nevertheless the reflections of the two propagation vectors seem to appear at the same temperature in the two compounds (figure 9).

We propose two alternative models: either both compounds order in a magnetic structure

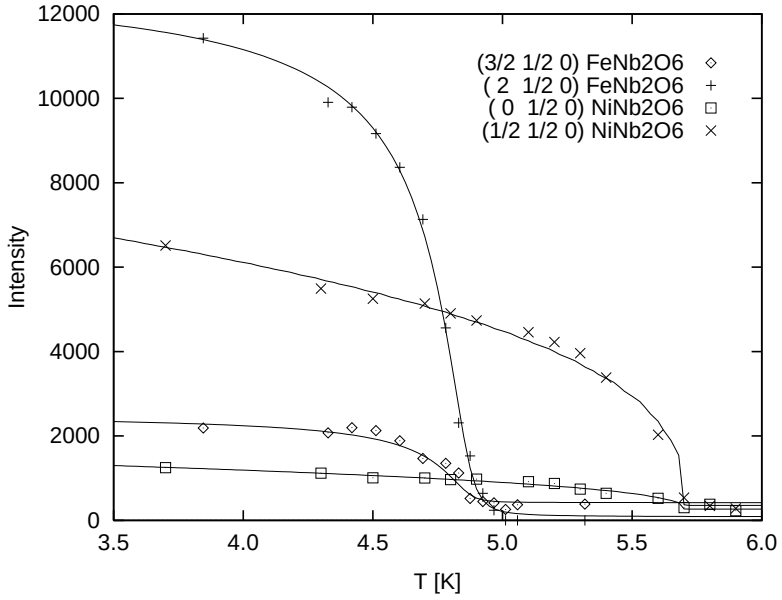

Figure 9. The temperature dependence of the intensities of some representative reflections in $FeNb_2O_6$ and $NiNb_2O_6$. Solid lines are guides to the eye.

with a fourfold unit cell and cell dimensions $2a \times 2b \times c$ which gives rise to the two propagation vectors, or two different magnetic domains exist in these compounds where each one results in only one propagation vector.

Attempts were made to fit the $FeNb_2O_6$ data to several models consistent with a fourfold magnetic unit cell. As no magnetic contributions to the nuclear peaks were observed, we were restricted to models with a translation symmetry according to the two observed propagation vectors. With the constraint that all magnetic sites have to be magnetically equivalent, no satisfactory fits were obtained. The only way to achieve reasonable agreement was to allow different absolute-moment values and different moment directions for Fe positions equivalent in the crystal structure.

In order to check this assumption, a Mössbauer spectrum at 4.2 K for $FeNb_2O_6$ powder was recorded, as magnetically different positions should result in different local hyperfine fields at the ^{57}Fe nuclei. The Mössbauer spectrum is very well reproduced by one set of parameters, with the asymmetry parameter η fixed to zero (figure 3). We found the angle $\Theta = 19.2 \pm 0.5^\circ$ between the direction of the hyperfine field and the principal axis of the electric field gradient at the iron nucleus. The quadrupole splitting $\frac{1}{2}e^2qQ$ was -2.36 ± 0.01 mm s^{-1}, the hyperfine field $H_{\rm hf}$ was 32.5 ± 0.1 kOe and the isomer shift IS relative to α-iron at room temperature was 1.26 ± 0.01 mm s^{-1}. These results are consistent with a previous experiment [14], but with smaller experimental errors.

Based on these results, the model with different magnetic positions has to be excluded. We therefore conclude that domains exist with two different magnetic structures corresponding to the two propagation vectors $(0\ \frac{1}{2}\ 0)$ and $(\frac{1}{2}\ \frac{1}{2}\ 0)$ in $FeNb_2O_6$. For the calculation of the absolute magnetic moment we assume the same value in the two domains. An F_xC_z-arrangement [5] with a canting angle of 23° to the a-axis and a moment of 4.5 μ_B was determined for $FeNb_2O_6$ at 1.3 K.

For $NiNb_2O_6$ we make the same assumption. But the reflections, according to the

Table 1. Atomic parameters for $FeNb_2O_6$ at 1.3 K obtained by powder diffraction; $a = 14.2367(16)$ Å, $b = 5.7322(3)$ Å, $c = 5.0433(3)$ Å, $\lambda = 2.5293$ Å, space group = $Pbcn$.

Atom	x	y	z
Fe	0	0.1657(12)	0.25
Nb	0.1632(6)	0.3199(10)	0.7509(25)
O(1)	0.0985(7)	0.3988(17)	0.4303(15)
O(2)	0.0817(6)	0.1182(19)	0.8952(15)
O(3)	0.2542(7)	0.1273(23)	0.5758(12)

Table 2. Atomic parameters for $NiNb_2O_6$ at 1.3 K obtained by powder diffraction; $a = 14.0140(19)$ Å, $b = 5.6825(3)$ Å, $c = 5.0244(3)$ Å, $\lambda = 2.5293$ Å, space group = $Pbcn$.

Atom	x	y	z
Ni	0	0.1602(9)	0.25
Nb	0.1591(3)	0.3215(7)	0.7468(26)
O(1)	0.0949(5)	0.3888(15)	0.4282(11)
O(2)	0.0787(4)	0.1081(16)	0.9046(10)
O(3)	0.2550(5)	0.1269(20)	0.5788(9)

Table 3. Magnetic moments of $FeNb_2O_6$ and $NiNb_2O_6$ at 1.3 K in the unit cell and the volume fractions of the domains obtained by powder diffraction.

Atom	$M(FeNb_2O_6)$	$M(NiNb_2O_6)$
$(0\ y\ \frac{1}{4})$	(1.82 0.0 4.15)	(1.32 0.0 2.03)
$(0\ \overline{y}\ \frac{3}{4})$	(1.82 0.0 4.15)	(1.32 0.0 2.03)
$(\frac{1}{2}\ \frac{1}{2} - y\ \frac{3}{4})$	(1.82 0.0 −4.15)	(1.32 0.0 −2.03)
$(\frac{1}{2}\ \frac{1}{2} + y\ \frac{1}{4})$	(1.82 0.0 −4.15)	(1.32 0.0 −2.03)
$(0\ \frac{1}{2}\ 0)$	91%	21%
$(\frac{1}{2} \pm\frac{1}{2}\ 0)$	9%	79%

propagation vector $(0\ \frac{1}{2}\ 0)$, cannot be included for refinement due to line broadening and the Lorentzian shape. Therefore we only adjusted the intensity of the $(0\ \frac{1}{2}\ 0)$ reflection to obtain an approximate value of the absolute magnetic moment under the assumption of equal values in the two domains and the same canting angle as in the $(\frac{1}{2}\ \frac{1}{2}\ 0)$ domain. We also found an F_xC_z-arrangement with a canting angle of 31° to the c-axis and a moment of 2.4 μ_B. The results of the refinement using powder data are given in tables 1–3. The observed and calculated diffraction patterns are shown in figures 1 and 2. The structures in both compounds related to the two propagation vectors agree with group theoretical considerations restricted to a Hamiltonian bilinear in the spin part. For the propagation vector $(0\ \frac{1}{2}\ 0)$ this was shown by Yaeger *et al* [8] and it can readily be transferred to the propagation vector $(\frac{1}{2}\ \frac{1}{2}\ 0)$.

To confirm our interpretation of the powder diffraction experiments we carried out a single-crystal experiment on $FeNb_2O_6$. The result of the refinement with the same domain model is given in tables 4 and 5. A different ratio of domains was observed for the single crystal, which confirms the domain model. The magnetic moment of 4.5 μ_B and a canting

Table 4. Magnetic moments of $FeNb_2O_6$ at 1.6 K in the unit cell and the volume fractions of the domains obtained by single-crystal diffraction.

Atom	$\boldsymbol{M}$
$(0\ y\ \frac{1}{4})$	(1.85 0.0 4.06)
$(0\ \bar{y}\ \frac{3}{4})$	(1.85 0.0 4.06)
$(\frac{1}{2}\ \frac{1}{2}-y\ \frac{3}{4})$	(1.85 0.0 −4.06)
$(\frac{1}{2}\ \frac{1}{2}+y\ \frac{1}{4})$	(1.85 0.0 −4.06)
$(0\ \frac{1}{2}\ 0)$	99.6%
$(\frac{1}{2}\ \frac{1}{2}\ 0)$	0.2%
$(\frac{1}{2}\ -\frac{1}{2}\ 0)$	0.2%

angle of 24° to the *a*-axis are in excellent agreement with the powder experiment.

The canting angles in these non-collinear magnetic structures are due to single-ion anisotropy of the M^{2+} ions which arises from the octahedral environment of the oxygen atoms. Thus the magnetic moment direction follows mainly the orientation of the oxygen octahedra. In $FeWO_4$ and $NiWO_4$ [15], with similar structures and with a similar orientation of oxygen octahedra relative to the cell axes, the moment directions are almost identical to those in our case. A canting angle of 27° to the *a*-axis was found in $FeWO_4$, and in $NiWO_4$ a canting angle of 32° relative to the *c*-axis was found.

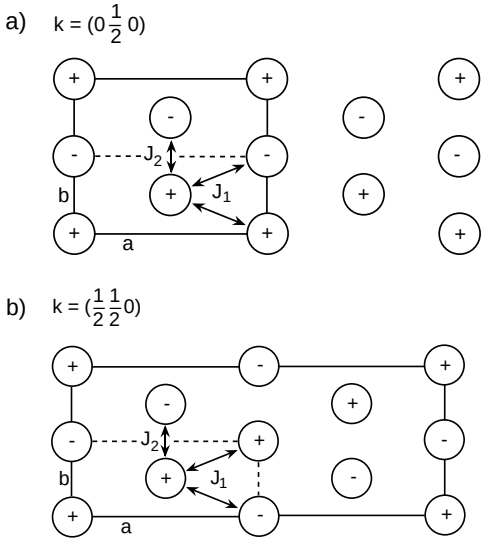

Figure 10. Projections of the two types of magnetic domain structure in $FeNb_2O_6$ onto the *a*–*b* plane. (a) shows the $(0\ \frac{1}{2}\ 0)$ structure, and (b) one of the two possibilities for the $(\frac{1}{2}\ \frac{1}{2}\ 0)$ structure. Solid lines give the magnetic elementary cell, dotted lines the nuclear one. Circles symbolize ions belonging to the same ferromagnetic zigzag chain, plus and minus signs indicate the orientation of the moments. J_1 and J_2 denote the effective interchain exchange.

In $FeNb_2O_6$ and $NiNb_2O_6$ the situation is similar to that for the isostructural compound $CoNb_2O_6$ [5] below 1.95 K. We find the same F_xC_z-arrangement of the moments indicating the same ferromagnetic zigzag chains along the *c*-direction. The intrachain coupling is

Table 5. Observed and calculated magnetic intensities of the $FeNb_2O_6$ single-crystal experiment at 1.5 K. $R = 0.048$.

h	k	l	F^2_{calc}	F^2_{obs}	h	k	l	F^2_{calc}	F^2_{obs}
0	1/2	0	354	343	1	1/2	0	236	241
1	−1/2	0	236	252	2	1/2	0	137	143
2	−1/2	0	137	151	0	1/2	1	87.4	87.7
0	1/2	1	87.4	90.4	0	−1/2	1	87.4	88.9
0	−1/2	1	87.4	75.2	−1	1/2	1	80.3	88.8
1	1/2	1	80.3	80.1	1	1/2	1	80.3	81.3
1	−1/2	1	80.3	80.3	3	1/2	0	96.2	99.4
3	−1/2	0	96.2	101	2	1/2	1	65.3	65.6
2	−1/2	1	65.3	69.3	0	3/2	0	1.0	0.8
0	−3/2	0	1.0	0.6	1	3/2	0	1.0	0.4
−1	3/2	0	1.0	0.3	−1	−3/2	0	1.0	0.1
1	−3/2	0	1.0	0.3	4	1/2	0	77.5	71.1
4	−1/2	0	77.5	71.7	2	3/2	0	0.8	0.6
−2	3/2	0	0.8	0.8	2	−3/2	0	0.8	0.7
−2	−3/2	0	0.8	0.5	3	1/2	1	51.1	50.2
3	−1/2	1	51.1	51.6	4	1/2	1	40.4	36.9
4	1/2	1	40.4	36.9	4	−1/2	1	40.4	38.7
1/2	1/2	0	1.1	1.1	−1/2	1/2	0	1.0	0.9
1/2	−1/2	0	1.0	1.1	−1/2	−1/2	0	1.1	1.1
3/2	1/2	0	0.9	0.8	−3/2	1/2	0	0.9	1.0
3/2	−1/2	0	0.9	1.1	−3/2	−1/2	0	0.9	0.9
5/2	1/2	0	0.4	0.5	−5/2	1/2	0	0.4	0.5
5/2	−1/2	0	0.4	0.4	−5/2	−1/2	0	0.4	0.5
1/2	1/2	1	0.3	0.3	1/2	−1/2	1	0.3	0.3
3/2	1/2	1	0.4	0.3	3/2	−1/2	1	0.4	0.4
7/2	1/2	0	0.3	0.1	7/2	−1/2	0	0.3	0.5
−7/2	1/2	0	0.3	0.5	−7/2	−1/2	0	0.3	0.2
1/2	3/2	0	0	0.2	−1/2	3/2	0	0	0.1
1/2	−3/2	0	0	0.1	−1/2	−3/2	0	0	0
5/2	1/2	1	0.2	0.1	5/2	−1/2	1	0.2	0.1
7/2	1/2	1	0.1	0	7/2	−1/2	1	0.2	0.4
1/2	3/2	1	1.2	1.0	1/2	−3/2	1	1.3	1.1
3/2	3/2	1	1.9	1.5	3/2	−3/2	1	1.9	2.0
5/2	3/2	1	1.0	1.0	−5/2	3/2	1	1.0	0.9
9/2	1/2	1	0.6	0.2	9/2	1/2	1	0.6	0.2
9/2	−1/2	1	0.6	0.6	9/2	−1/2	1	0.6	0.1
11/2	1/2	0	0.2	0.3	11/2	−1/2	0	0.2	0.2

based on 90° superexchange, whereas interchain coupling has to overcome at least four bond lengths for chains in the same *b*–*c* layer and six bond lengths to chains in other layers. Therefore the coupling in the chains is assumed to be ferromagnetic and considerably stronger than the interchain exchange. The coupling between the ferromagnetic chains in the *b*-direction is thus antiferromagnetic. For the succession in the *a*-direction three possible stacking schemes exist and give rise to the two observed propagation vectors (figure 10). Neglecting the exchange interaction with moments in the next-nearest layer of magnetic ions, separated by the distance of the lattice parameter *a*, the exchange energies in the two cases are exactly the same. As the exchange interaction over 14 Å (this is more than 12 bonds) is negligible and the dipole–dipole interaction has no preference for one possibility, frustration results. Already dislocations, causing local strain or surface effects, could prefer one or the other stacking scheme and produce domains. Thus in the $FeNb_2O_6$ single crystal

with a negligible surface the domains decorated by a propagation vector ($\frac{1}{2}$ $\frac{1}{2}$ 0) nearly vanish. In the $NiNb_2O_6$ powder the magnetic order with a propagation vector (0 $\frac{1}{2}$ 0) seems to be of short range as indicated by the broadening of magnetic reflections for larger 2Θ, indicating the small size of domains in this structure.

These niobates with columbite structure are comparable to $FeC_2O_4{\cdot}2D_2O$ [16]. This compound is characterized by a strong antiferromagnetic intrachain and weaker interchain coupling, which exhibits two types of stacking. But in $FeC_2O_4{\cdot}2D_2O$ with $T_N = 11.7$ K the ordered moments switch partially at $T_2 = 9.5$ K to the other structure, perhaps because of magnetoelastic interaction. In $FeNb_2O_6$ and $NiNb_2O_6$ the structures of the two propagation vectors order at the same temperature, and the powder diffraction measurements at different temperatures show no change of the ratio between the two domains.

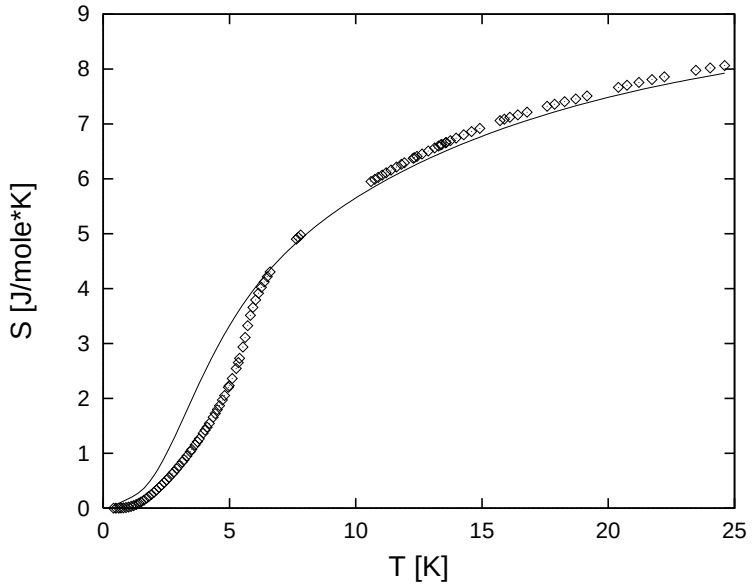

Figure 11. Magnetic entropy of $NiNb_2O_6$ obtained by numerical integration. The solid line gives the theoretical prediction for a ferromagnetic Heisenberg chain with single-ion anisotropy.

The dominant role of the intrachain coupling in $NiNb_2O_6$ is also deduced from the specific heat data measured on a single crystal (figure 4). We estimate the specific heat of the non-magnetic isostructural $ZnNb_2O_6$ to be a good approximation of the lattice contribution in $NiNb_2O_6$. So the magnetic part of the specific heat was obtained by subtracting the $ZnNb_2O_6$ specific heat as measured by Hanawa *et al* [17]. The long tail of the magnetic specific heat above T_N reveals the presence of short-range magnetic correlations characteristic for low-dimensional magnetic behaviour. Figure 11 shows that the entropy of an $S = \frac{1}{2}$ ion is reached at 10 K and therefore single-ion anisotropy is not very strong. Therefore theoretical predictions for a ferromagnetic $S = 1$ chain with isotropic exchange coupling and uniaxial single-ion anisotropy [18] were fitted to the specific heat data. As a linear chain shows no three-dimensional ordering, only data between 10 K and 25 K were taken into account to describe the effect of short-range magnetic correlations above T_N. The important role of short-range magnetic correlations is emphasized by the fact that up to T_N only 25% of the entropy is acquired. The best agreement was obtained with the exchange parameter

$J = 14.8$ K and the single-site anisotropy $D = -5.2$ K. In the high-temperature region the magnetic entropy fits well to the theoretical prediction. The $S = 1$ triplet ground state, usually observed for a $3d^8$ ion in an octahedral symmetry, is therefore split by a crystal field of lower symmetry into a singlet and a ground doublet. The interchain interactions responsible for the three-dimensional ordering in the compound are weaker and can be estimated [19] using T_N. Depending on the degree of anisotropy the interchain exchange parameter yields $J' = 0.01$ K to 2.1 K corresponding to the limiting cases of an Ising or classical spin system.

4. Analysis

In previous publications analyses of the magnetic susceptibilities of $FeNb_2O_6$ [7] and $NiNb_2O_6$ [8] based on effective spin Hamiltonians were reported. A collinear magnetic structure was assumed, especially for $NiNb_2O_6$, in contrast to our neutron diffraction results. However, the new neutron diffraction results show that single-ion anisotropy exists and has a non-negligible influence causing a canting angle and an obvious unquenched orbital momentum. Based on these results a more detailed analysis taking into account the degrees of freedom in orbital angular momentum is presented.

According to Hund's rules the $3d^6$ electron configuration of Fe^{2+} results in a ^5D ground state. The first excited state ^4P is separated by $\sim 30\,000$ cm^{-1} and can therefore be neglected [20]. The ^5D free-ion ground state of Fe^{2+} splits into an orbital triplet $^5T_{2g}$ and an orbital singlet ^5E_g in a crystal field of cubic symmetry. The triplet ($^5T_{2g}$) is of lowest energy. Within this triplet the splitting is of the order of 1000 cm^{-1} so the other orbital states do not contribute to magnetic properties significantly. The lowest triplet is therefore an adequate approximation for the calculations, spanned by

$$\psi_1 = \sqrt{15}yz \qquad \psi_2 = \sqrt{15}xz \qquad \psi_3 = \sqrt{15}xy.$$

These functions transform under rotation like those of the orbital angular momentum with $L = 1$:

$$L_x = \kappa\begin{pmatrix} 0 & 0 & 0 \\ 0 & 0 & \mathrm{i} \\ 0 & -\mathrm{i} & 0 \end{pmatrix} \qquad L_y = \kappa\begin{pmatrix} 0 & 0 & -\mathrm{i} \\ 0 & 0 & 0 \\ \mathrm{i} & 0 & 0 \end{pmatrix} \qquad L_z = \kappa\begin{pmatrix} 0 & \mathrm{i} & 0 \\ -\mathrm{i} & 0 & 0 \\ 0 & 0 & 0 \end{pmatrix}.$$

The covalency factor κ reflects the influence of higher states whose effects are assumed to be isotropic [20]. In a first step this parameter was fixed to 1. It is a suitable test for the restriction to the lower triplet.

In $NiNb_2O_6$ the situation is more complicated. The free-ion ground state ^3F splits in a crystal field of cubic symmetry into two triplets $^3T_{1g}$, $^3T_{2g}$ and a low-lying orbital singlet $^3A_{2g}$. But also an orbital singlet ^1E_g of the next excited free-ion state ^1D can be of similar energy to the $^3T_{2g}$ state [21]. We will restrict consideration to the ground singlet $^3A_{2g}$ and the triplet $^3T_{2g}$ to reproduce an anisotropy of orthorhombic symmetry. The basis functions are

$$\chi = \sqrt{105}xyz \qquad \psi_1 = \frac{1}{2}\sqrt{105}x(y^2 - z^2)$$
$$\psi_2 = \frac{1}{2}\sqrt{105}y(z^2 - x^2) \qquad \psi_3 = \frac{1}{2}\sqrt{105}z(x^2 - y^2).$$

The matrix elements of the orbital momentum operator for these functions are

$$L_x = \begin{pmatrix} 0 & 2\mathrm{i} & 0 & 0 \\ -2\mathrm{i} & 0 & 0 & 0 \\ 0 & 0 & 0 & -\mathrm{i}/2 \\ 0 & 0 & \mathrm{i}/2 & 0 \end{pmatrix}$$

$$L_y = \begin{pmatrix} 0 & 0 & 2\mathrm{i} & 0 \\ 0 & 0 & 0 & \mathrm{i}/2 \\ -2\mathrm{i} & 0 & 0 & 0 \\ 0 & -\mathrm{i}/2 & 0 & 0 \end{pmatrix}$$

$$L_z = \begin{pmatrix} 0 & 0 & 0 & 2\mathrm{i} \\ 0 & 0 & -\mathrm{i}/2 & 0 \\ 0 & \mathrm{i}/2 & 0 & 0 \\ -2\mathrm{i} & 0 & 0 & 0 \end{pmatrix}.$$

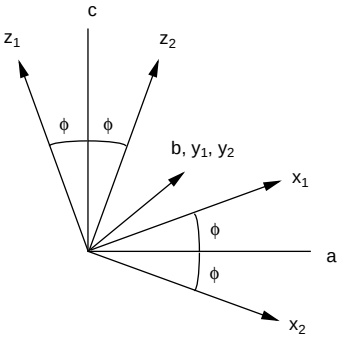

Figure 12. Local principal axes x_i, y_i, z_i of the g-tensor of the magnetic ions occupying the two types of magnetically non-equivalent site in MNb_2O_6 (M = Fe, Ni). a, b and c are the crystallographic axes.

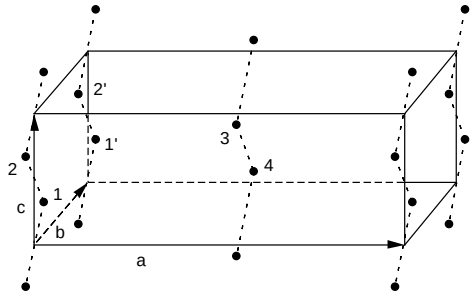

Figure 13. Indexed magnetic ions in the chemical unit cell.

As the M^{2+} ion is situated on a twofold axis along [010], the crystal-field Hamiltonian can be written as

$$H_{\text{crystal field}} = B_2^0 O_2^0 + B_2^1 O_2^1 + B_2^2 O_2^2 + B_4^0 O_4^0 + B_4^1 O_4^1 + B_4^2 O_4^2 + B_4^3 O_4^3 + B_4^4 O_4^4$$

by the use of Stevens operators. No operator mixes ψ_2 with ψ_1 or ψ_3, but ψ_1 and ψ_3 can be mixed. Instead of using a mixing parameter, we introduce a principal-axes system, which is related to the crystal axes system by a rotation around the b-axis at each magnetic site, as shown in figure 12. Only three parameters are needed instead of eight in the general case to describe the effects of a crystal field in the case of $FeNb_2O_6$. These are $E(\psi_2) - E(\psi_1)$, $E(\psi_3) - E(\psi_1)$ and ϕ for the transformation angle between the principal-axes and crystal axes systems. In the case of $NiNb_2O_6$ two additional parameters are required. These are $E(\psi_1) - E(\chi)$ and δ for the mixing between ψ_2 and χ. The crystal-field eigenstates become

$$\chi' = \cos(\delta)\chi - \sin(\delta)\psi_2 \qquad \psi_2' = \sin(\delta)\chi + \cos(\delta)\psi_2.$$

Thus $H_{\text{crystal field}}$ is no longer diagonal in the principal-axes system:

$$H^{\mathrm{Ni}^{2+}}_{\text{crystal field}} = \begin{pmatrix} \sin(\delta)^2 E(\psi_2) & 0 & \sin(\delta)\cos(\delta)E(\psi_2) & 0 \\ 0 & E(\psi_1) & 0 & 0 \\ \sin(\delta)\cos(\delta)E(\psi_2) & 0 & \cos(\delta)^2 E(\psi_2) & 0 \\ 0 & 0 & 0 & E(\psi_3) \end{pmatrix}.$$

The full Hamiltonian can be taken as

$$H = H_{\text{crystal field}} + H_{\text{spin–orbit}} + H_{\text{exchange}} + H_{\text{magnetic dipole–dipole}} + H_{\text{Zeeman}}.$$

With the standard representation for the spin quantized in the principal-axes system as well we have

$$H_{\text{spin–orbit}} = \lambda \boldsymbol{L} \cdot \boldsymbol{S}.$$

In a free Fe^{2+} ion the spin–orbit coupling constant is $\lambda = -103$ cm^{-1} [20], and it is $\lambda = -324$ cm^{-1} for a Ni^{2+} ion [21]. The absolute value of λ can be slightly decreased under the action of a crystal field. The Zeeman term is given by

$$H_{\text{Zeeman}} = -\mu_B(2\boldsymbol{S} + \boldsymbol{L}) \cdot \boldsymbol{H}_{ext}$$

and the two many-particle interactions will be treated in the mean-field approximation:

$$H_{\text{exchange}} = -\sum_{\langle i,j \rangle} J_{ij} \boldsymbol{S}_i \langle \cdot \boldsymbol{S}_j \rangle_T$$

and

$$H_{\text{magnetic dipole–dipole}} = \frac{1}{4\pi\mu_0} \sum_{\langle i,j \rangle} \left(\frac{\boldsymbol{\mu}_i \cdot \langle \boldsymbol{\mu}_j \rangle}{r_{ij}^3} - 3\frac{(\boldsymbol{\mu}_i \cdot \boldsymbol{r}_{ij})(\langle \boldsymbol{\mu}_j \rangle \cdot \boldsymbol{r}_{ij})}{r_{ij}^5} \right).$$

In calculating these two terms we applied the translational symmetry of the magnetic structure which is the same for the observed magnetic domains. Structural data are taken from tables 1 and 2. The model parameters are the intrachain exchange J_0 $(=J_{12})$, the interchain exchange to the four neighbour chains in the next layers in the a-direction J_1 $(=J_{13} + J_{14} = J_{23} + J_{24})$ and the interchain exchange to the next two chains in the same layer in the b-direction J_2 $(=J_{11'} + J_{12'} = J_{21'} + J_{22'})$ with respect to the notation of the ions as given in figures 10 and 13. This simplification is justified by the weak interchain exchange as explained above.

The iteration is started with a randomly chosen set of parameters. All of the calculations were carried out in the principal-axes system. After diagonalization of the Hamiltonian the thermal expectation values were calculated and reinjected into the iteration. This procedure was repeated until self-consistency was achieved.

In order to determine the model parameters the following experimental data have been used.

(i) The susceptibilities with an external field applied along one of the crystal axes a, b and c in the temperature range from 30 to 300 K. Above 30 K the susceptibility obeys a Curie–Weiss law.

(ii) The magnetization in the ordered state with an external field applied along the a- or c-axis at 2 K in the field range from 1 to 5 T.

From our data we conclude that for both compounds for two directions of the applied external field, a and c, a field-induced transition to the paramagnetic state takes place. The critical field strengths at 2.0 K are $H_{\text{cr}}^a = 9.0$ kOe and $H_{\text{cr}}^c = 18.5$ kOe for $FeNb_2O_6$ and $H_{\text{cr}}^a = 27.8$ kOe and $H_{\text{cr}}^c = 10.5$ kOe for $NiNb_2O_6$. The magnetic structure of the antiferromagnetic phase and the simulated structures of the high-field states are shown in figure 14. In the high-field state the spin configurations can be assigned as F_xC_z for the field applied along the a-direction, and C_xF_z for the field applied along the c-direction, where the propagation vectors are (0 0 0) in any case. Thus the ferromagnetic chain structures along the c-direction are preserved. Effective exchange interactions were sufficient for the description of the observed phase transitions.

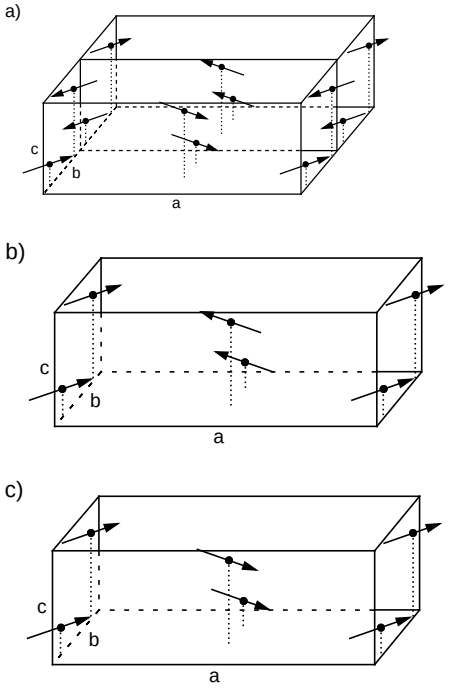

Figure 14. Magnetic structures in the case of $FeNb_2O_6$ for (a) the antiferromagnetic phase, (b) the high-field state with a field applied along the *c*-axis and (c) with a field applied along the *a*-axis. All of the magnetic moments lie in the *a*–*c* plane.

Table 6. Physical parameters for the best agreement for $FeNb_2O_6$ and $NiNb_2O_6$.

Parameter	$FeNb_2O_6$	$NiNb_2O_6$
λ	-99 cm^{-1}	-208 cm^{-1}
$E(\Psi_2) - E(\Psi_1)$	182 cm^{-1}	-187 cm^{-1}
$E(\Psi_3) - E(\Psi_1)$	540 cm^{-1}	-408 cm^{-1}
$E(\Psi_1) - E(\chi)$		4972 cm^{-1}
δ		0.01
ϕ	65.9°	39.2°
J_0	1.76 K	9.86 K
J_1	-0.095 K	-0.43 K
J_2	-0.62 K	-1.07 K

The best agreement with our data was found for the parameters given in table 6. The deviation of the covalency factor κ, introduced for the Fe^{2+} ion, is less than 5% and therefore not significant. The results of the refinement are displayed in figures 5–8.

As usual in mean-field calculations the Néel temperatures are higher than the experimental values. They were not included into the refinement and give 16.2 K for $FeNb_2O_6$ and 15.6 K for $NiNb_2O_6$. For $FeNb_2O_6$ the anisotropy can be expressed in the principal-axes system [22] as: $D^{xx} = 0$, $D^{yy} = -18$ cm^{-1}, and $D^{zz} = -54$ cm^{-1} or $g^{xx} = 2.0$, $g^{yy} = 2.37$, and $g^{zz} = 3.09$. This reveals a strong uniaxial anisotropy and a quasi-Ising character for the spin system. The simulation gives a value of 4.5 μ_B for the fully ordered magnetic moment and a canting angle of 24.2° to the *a*-axis in good

agreement with the neutron diffraction results. For $NiNb_2O_6$ we found $D^{xx} = -34.7$ cm^{-1}, $D^{yy} = -36.1$ cm^{-1}, and $D^{zz} = -37.8$ cm^{-1} or $g^{xx} = 2.33$, $g^{yy} = 2.35$, and $g^{zz} = 2.36$ and thus a much weaker anisotropy. The ordered magnetic moment was 2.3 μ_B, and a canting angle of 36.4° to the *c*-axis compared with 31° from neutron diffraction was obtained. The agreement with the specific heat data is satisfying, where we obtained $J = 14.8$ K and $D = -5.2$ K as compared to $J_0 = 9.9$ K and $D^{zz} - D^{xx} = -4.5$ K in our analysis.

Deviations of the magnetization curves from the experimental findings might be due to the fact that we employed effective exchange interactions. Thus the ions in one zigzag chain can be treated as equal, but in general exchange from one ion in one chain to members in another chain may be different giving rise to an additional spin deviation between spins in one chain. This effect should be more important in $NiNb_2O_6$ than in $FeNb_2O_6$ because the single-ion anisotropy is weaker there. A strong anisotropy fixes the moments in one direction which is the same for all ions in one zigzag chain. Nevertheless the neutron diffraction results give no evidence of an additional G_xA_z-component to the F_xC_z-configuration [5] for $NiNb_2O_6$ as well as for $FeNb_2O_6$.

5. Conclusion

From neutron diffraction experiments we were able to determine the magnetic structures of $FeNb_2O_6$ and $NiNb_2O_6$. The two compounds order in the same type of magnetic structure, where due to frustration three domain types can exist and give rise to two different propagation vectors. This model was confirmed for $FeNb_2O_6$ by a Mössbauer experiment and does also agree with group theory.

We have shown that the magnetic behaviour of $FeNb_2O_6$ and $NiNb_2O_6$ can be well explained in mean-field approximation in the ordered and the paramagnetic state. Neutron diffraction results were not used, but agree with structures obtained using the model mentioned and a parameter set satisfying the magnetization data. In both cases an orthorhombic anisotropy was found, which is weaker in $NiNb_2O_6$. Even if the high-temperature paramagnetic susceptibility of $NiNb_2O_6$ single crystals exhibits no pronounced anisotropy, magnetization measurements and neutron diffraction studies at low temperatures show that the influence of single-ion anisotropy cannot be neglected.

The crystal-field levels of Fe^{2+} in $FeNb_2O_6$ are found to be different from those obtained by Yaeger *et al* [8] and Eibschütz *et al* [23]. Agreement was only found as regards the fact that the lowest-lying triplet $^5T_{2g}$ is well separated from the higher levels, and therefore population of higher levels can be neglected at sufficiently low temperatures. As the magnetization in the high-field state is very well simulated, we place reliance on our results rather than on results obtained only from susceptibility data. In $NiNb_2O_6$ only the splitting of the crystal-field ground term can be given with good accuracy. From the relatively weak anisotropy in the magnetization at high temperatures it is hardly possible to obtain reliable values for the spin–orbit coupling constant and the overall splitting of the orbital triplet $^3T_{2g}$ and singlet $^3A_{2g}$, or to decide whether the orbital singlet ^1E_g is involved or not. The Ni^{2+} level scheme could be better checked by optical methods. Nevertheless the higher crystal-field levels seem to be well separated from the orbital ground singlet.

The ordered magnetic moments of both compounds lie in the *a*–*c* plane on either side of the crystallographic *z*-axis following the local easy axis of the ion. The simulated ordered magnetic moments agree very well with our experimental results. Deviations are within experimental errors.

In both compounds the ferromagnetic superexchange in the chains along the *c*-direction is the strongest interaction. The interchain exchange interaction was found to be smaller

and antiferromagnetic. This results in a low-dimensional behaviour that was observed for example in the specific heat experiment on $NiNb_2O_6$. A specific heat experiment on $FeNb_2O_6$ should also reveal a similar effect but with a more pronounced Ising-like behaviour. However, the decrease of dimensionality should not be as strong as in the isostructural compound $CoNb_2O_6$, as was observed by Hanawa *et al* [17]; an estimation of the interchain exchange parameters in this compound was given in a previous publication [5].

Acknowledgments

The authors are grateful to J P Sanchez and J L Oddon for their assistance in recording the Mössbauer spectra. The hospitality and the kind help of the CENG/MDN in the performance of the neutron diffraction experiments and magnetization measurements are also gratefully acknowledged. This work was supported by the Bundesminister für Bildung und Forschung under Contracts No 03WL2DAR8, No 3FU3DAR and No 03WE4DAR5.

References

[1] Weitzel H 1976 *Z. Kristallogr.* **144** 238
[2] Weitzel H 1971 *Z. Anorg. Allg. Chem.* **380** 119
[3] Klein S and Weitzel H 1976 *Acta Crystallogr.* A **32** 587
[4] Nielsen O V, Lebech B, Krebs Larsen F, Holmes L M and Ballman A A 1976 *J. Phys. C: Solid State Phys.* **9** 2401
[5] Heid C, Weitzel H, Burlet P, Bonnet M, Gonschorek W, Vogt T, Norwig J and Fuess H 1995 *J. Magn. Magn. Mater.* **151** 123
[6] Weitzel H 1976 *Acta Crystallogr.* A **32** 592
[7] Yaeger I, Morrish A H and Wanklyn B M 1977 *Phys. Rev.* B **15** 1465
[8] Yaeger I, Morrish A H, Wanklyn B M and Garrard B J 1977 *Phys. Rev.* B **16** 2289
[9] Schröcke H 1966 *Neues Jahrb. Mineralog. Abh.* **106** 1
[10] Rodriguez-Carvajal J 1990 *Satellite Mtg of the 15th Congr. of the International Union of Crystallography (Toulouse)* abstracts, p 127
[11] Wanklyn B M, Garrard B J and Garton G 1976 *Mater. Res. Bull.* **11** 1497
[12] Becker P and Coppens P 1974 *Acta Crystallogr.* A **30** 129
[13] Elsenhans O 1990 *J. Appl. Crystallogr.* **23** 73
[14] Yaeger I, Morrish A H, Boumford C, Wong C P, Wanklyn B M and Garrard B J 1978 *Solid State Commun.* **28** 651
[15] Weitzel H and Langhof H 1977 *J. Magn. Magn. Mater.* **4** 265
[16] Simizu S, Chen J, Friedberg S, Martinez J and Shirane G 1987 *J. Appl. Phys.* **61** 3420
[17] Hanawa T, Ishikawa M and Miyatani K 1992 *J. Phys. Soc. Japan* **61** 4287
[18] Blöte H W J 1975 *Physica* B **79** 427
[19] Steiner M, Villain J and Windsor C G 1976 *Adv. Phys.* **25** 87
[20] Abragam A and Pryce M H L 1951 *Proc. R. Soc.* A **206** 173
[21] Orgel L E 1955 *J. Chem. Phys.* **23** 1005
[22] Pryce M H L 1950 *Proc. Phys. Soc.* A **63** 25
[23] Eibschütz M, Ganiel U and Shtrikman S 1967 *Phys. Rev.* **156** 259